Wireless Netw (2019) 25:689–698
https://doi.org/10.1007/s11276-017-1585-z

Cooperative decode-and-forward quadrature spatial modulation over correlated and imperfect η–μ fading channels

Saud Althunibat[1] · Raed Mesleh[2]

Published online: 20 September 2017

Abstract This paper analyzes the performance of quadrature spatial modulation (QSM) multiple-input multiple-output (MIMO) system in cooperative decode and forward (DF) networks over correlated and imperfect η–μ fading channels. QSM is a recently proposed propitious MIMO technique that promises significant advantages over conventional MIMO schemes including high spectral efficiency with single RF-chain transmitter and very low receiver complexity. In this study, DF cooperative communication system adopting QSM technique is presented and throughly analyzed. Single or multiple DF relays are placed between the source and the destination to cooperate in the transmission process. Only the relays that decode the signal correctly will participate in the retransmission process. The end to end performance of the considered system is analyzed over correlated and imperfect η–μ fading channels. The η–μ channel is a general fading distribution that includes some other well-known channels, such as Rayleigh and Nakagami-m, as spacial cases. Monte Carlo simulation results are presented to corroborate the accuracy of the conducted analysis. The impact of spatial correlation, imperfect channel estimation and the fading parameters η and μ on the overall performance is investigated and exhaustively discussed.

✉ Saud Althunibat
saud.althunibat@ahu.edu.jo

Raed Mesleh
raed.mesleh@gju.edu.jo

1 Department of Communications Engineering, Al-Hussein Bin Talal University, P.O. Box 20, Ma'an, Jordan

2 School of Electrical Engineering and Information Technology, German Jordanian University, Amman–Madaba Street, P.O. Box 35247, Amman 11180, Jordan

Keywords MIMO · Quadrature spatial modulation (QSM) · Cooperative networks · Decode and forward relay networks · Performance analysis

1 Introduction

Wireless communication in its current form spans over a wide range of applications including software, hardware, Internet, cellular and related services and development. Future wireless standards, such as 5G and beyond, target huge data rate, very low end-to-end latency communication, huge reduction in power consumption, and smart systems and applications. Researchers and industry worldwide are looking for new technologies and improved systems. At the same time, an explosion in wireless data transmission through smart devices is witnessed in the past few years. Among the several investigated techniques for 5G, collaborative and distributed signal processing techniques, such as cooperative communication and multiple input multiple output (MIMO) systems, promise significant energy saving and performance gain [1].

A recently proposed MIMO scheme called *quadrature spatial modulation (QSM)* forebodes significant advantages in terms of data rate, energy efficiency, hardware cost and receiver complexity [2]. As such, combining QSM with cooperative networks promises several advantages that are appealing for future wireless systems. In a QSM system, an additional quadrature spatial constellation diagram is utilized to enhance the spectral efficiency of conventional spatial modulation (SM) [3] system. As such, a system with N_t transmit antennas and M modulation order, can deliver a bit block of $\log_2 N_t^2 M$ bits at each transmission instant. At the same time and even though multiple transmit antennas exist, only single RF chain is needed,which diluted energy efficiency and hardware cost, and the computational complexity at the receiver remains as low as that of conventional SM. , where an additional base two logarithm of the number of transmit antennas is achieved as compared to SM [2].

Based on its unique modulation concept and the very promising assets, QSM attracted momentum research interest [4]. A low-complexity detectors for QSM were proposed with nearly negligible performance loss in [5]. In [6], the performance of QSM is analyzed and evaluated in cognitive radio networks under the presence of channel estimation errors and limited feedback. The impact of co-channel interference and channel estimation errors on the performance of QSM over Rayleigh fading channels are respectively investigated in [7] and [8]. The QSM performance over Nakagami-m fading channels is studied in [9] and over correlated and imperfect generalized fading channels in [10]. Besides, QSM has been considered to enhance the performance of conventional cooperative communication systems. In [11], a multi-antenna source applying QSM technique is communicating with a single antenna destination and multiple single antenna amplify and forward (AF) relays participate in the transmission process. An upper bound on the average bit error rate (BER) performance is derived and discussed. The performance of AF cooperative spectrum-sharing systems applying QSM technique is investigated in [12]. Specifically, secondary users are communicating with the help of an AF relay over a spectrum shared with multiple primary users and a tight upper bound of the BER performance over Rayleigh fading channel is obtained. Lately, a study similar to [11] is presented in [13] by considering decode and forward (DF) relays instead of AF ones.

This paper contributes to existing theory by studying the performance of a cooperative communication system over spatially correlated and imperfect generalized η–μ fading channels. To the best of the authors knowledge, performance analysis of cooperative MIMO systems over such generalized channels does not exist in literature. In fact, obtaining the probability distribution function (PDF) of the SNR at the receiver input over such channels is mathematically involved and intractable. In this work, we propose a novel derivation that doesn't require the PDF of the SNR and it is shown to be very accurate for wide range of system parameters. The study considers a source, destination and multiple DF relays all equipped with multiple antennas. A QSM signal is generated and transmitted by the source in the first time slot. The DF relays decode the source signal and only those relays that detect the signal correctly will be allowed to participate in the retransmission process during a second time slot. The destination combines all received signals over the two time slots to retrieve the original data bits. The average pair wise error probability (PEP) performance of the system under study is derived and used to obtain a tight upper bound on the average BER. The impact of different system and channel parameters on the overall performance is investigated and thoroughly discussed. A practical model is considered in which the channel statistics are estimated at the relays and the destination. In addition, deploying multi-antennas generally induces spatial correlation among different channel paths, which is investigated here as well.

The η–μ fading channel is a general fading distribution that describes the small scale variations of a propagation signal in a non-line-of-sight environment. As such, it permits the modeling of other famous distributions as special cases. The Hoyt distribution can be obtained by setting $\eta = q^2$ and $\mu = 1/2$. The Nakagami-m is realized when $\eta = 1$ and $\mu = m/2$. Rayleigh fading is obtained when $\eta = 1$ and $\mu = 1/2$. Also, the one-sided Gaussian distribution is configured when $\eta = 1$ and $\mu = 1/4$ [14].

In summary and with reference to existing literature, the main contributions of this paper are three folds. (1) DF cooperative communication system applying QSM modulation technique at all transmitting nodes is considered. (2) The end to end performance is analytically analyzed and verified through Monte Carlo simulations assuming generalized η–μ fading channel distribution. (3) The impact of channel correlation and imperfect channel estimation on the overall performance is studied.

The rest of the paper is organized as follows. The system and channel models are presented in Sect. 2. Performance analysis is derived in Sect. 3. Analytical and simulation results are throughly discussed in Sect. 4. Conclusions and future directions are drawn in Sect. 5.

2 System and channel models

A cooperative MIMO wireless communication system is considered in this study as depicted in Fig. 1. A source equipped with N_t antennas communicates with a destination that has N_r receive antennas and R DF relays each with L_t transmit and L_r receive antennas cooperate in the communication protocol. A transmitted signal from the source is received by the destination and the relays in the first phase. The relays decode the source message and only those relays that detect the signal correctly are allowed to participate in the second transmission phase. To facilitate this, it is assumed that each relay is able to incisively detect any errors that might occur in the received data. Such receiver is generally called a genie aided receiver and it can be considered as an upper bound to any practical receivers. In functional DF systems, error detection techniques need

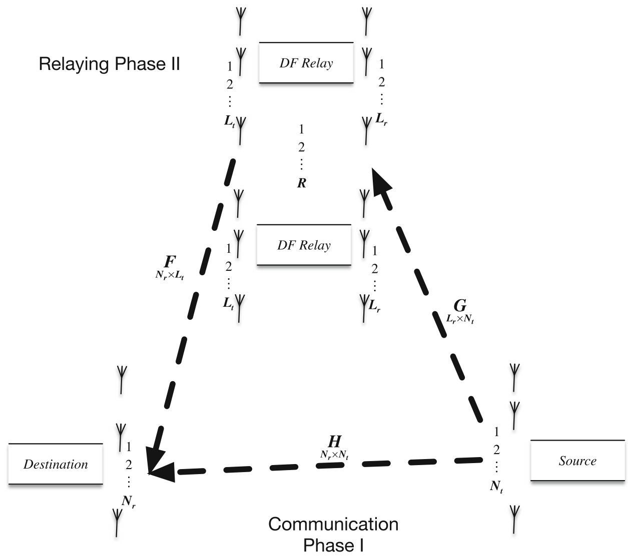

Fig. 1 DF Cooperative QSM system model assuming a source with N_t antennas communicating with a destination that has N_r receive antennas and R DF relays each with L_t transmit and L_r receive antennas cooperate in the communication protocol

to be considered. Yet, the assumed simplification in this paper is required to facilitate mathematical derivation and is commonly assumed in the literature [15–17].

In the first communication phase, the source broadcasts the message that is received by the destination node and the relays. Let $\mathbf{H}$ denotes the $N_r \times N_t$ MIMO channel matrix between the source and the destination as illustrated in Fig. 1. The entries of $\mathbf{H}$ are assumed to be independent and identically distributed (i.i.d) random variables that follow the generalized η–μ fading model [14]. In addition, spatial correlation among transmit and receive antennas is assumed, which generally occurs due to insufficient spatial separation between antenna elements. Assuming antennas are vertically aligned, the correlation coefficients among source and destination antennas are given by ρ_s and ρ_d, respectively. Hence, the modified channel model in the presence of spatial correlation, $\tilde{\mathbf{H}}$, can be formulated according to Kronecker model [18] as

$$\tilde{\mathbf{H}} = \mathbf{R}_d^{\frac{1}{2}}\mathbf{H}\mathbf{R}_s^{\frac{1}{2}}, \tag{1}$$

where $\mathbf{R}_s$ and $\mathbf{R}_d$ respectively represent the correlation matrices at the source and the destination. The correlation matrices can be generated using the the exponential decay model as $\mathbf{R}_s(i,j) = \rho_s^{|i-j|}$ where $1 \leqslant i\&j \leqslant N_t$ and $\mathbf{R}_d(i,j) = \rho_d^{|i-j|}$ with $1 \leq i\&j \leq N_r$ [19]. The general correlation model at both sides can be written as $\mathbf{R}_H = \mathbf{R}_s \otimes \mathbf{R}_d$, which simplifies (1) to [18]

$$\mathrm{vec}(\tilde{\mathbf{H}}) = \mathbf{R}_H^{\frac{1}{2}}\mathrm{vec}(\mathbf{H}) \tag{2}$$

In this study, each DF relay is assumed to be equipped with multiple antennas and spatial correlation is preset at the relay node as well. The entries of the channel matrix between the source and the i th relay $(1 \leqslant i \leqslant R)$, denoted by $\tilde{\mathbf{G}}^{(i)}$, and the channel matrix between the i th relay and the destination, denoted by $\tilde{\mathbf{F}}^{(i)}$, follow a correlated $\eta - \mu$ fading channel model as discussed before. The spatial correlation on $\tilde{\mathbf{G}}^{(i)}$ and $\tilde{\mathbf{F}}^{(i)}$ can be respectively modeled as

$$\tilde{\mathbf{G}}^{(i)} = \mathbf{R}_{rr}^{\frac{1}{2}}\mathbf{G}^{(i)}\mathbf{R}_s^{\frac{1}{2}} \tag{3}$$

$$\tilde{\mathbf{F}}^{(i)} = \mathbf{R}_d^{\frac{1}{2}}\mathbf{F}^{(i)}\mathbf{R}_{rt}^{\frac{1}{2}}. \tag{4}$$

The matrices $\mathbf{R}_{rt}$ and $\mathbf{R}_{rr}$ respectively denote the spatial correlation matrices at the relay transmit and receive antennas. Specifically, $\mathbf{R}_{rt}$ is an $L_t \times L_t$ square matrix whose entries $\mathbf{R}_{rt}(i,j) = \rho_{rt}^{|i-j|}$ for $1 \leq i\&j \leq L_t$, and $\mathbf{R}_{rr}$ is an $L_r \times L_r$ square matrix whose entries $\mathbf{R}_{rr}(i,j) = \rho_{rr}^{|i-j|}$ for $1 \leq i\&j \leq L_r$. Besides, ρ_{rt} and ρ_{rr} respectively represent the relay transmit and receive correlation coefficients.

2.1 First transmission phase

At each time instant, $\log_2\left(N_t^2 M_s\right)$ bits are modulated through a QSM modulator and transmitted from the source, with M_s being the modulation order employed. In a QSM system, each bits block is partitioned into three sub-blocks. The first sub-block includes $\log_2 M_s$ bits, which modulate a signal modulation symbol from arbitrary quadrature amplitude modulation (QAM)/phase shift keying (PSK) constellation diagram. The modulated complex symbol, $x = xR + jxI$, $x \in \{1 : M_s\}$, is decomposed into it's in-phase, $x_{\Re}$, and quadrature components, $x_{\Im}$. The other sub-blocks each with $\log_2 N_t$ bits modulate two spatial constellation symbols. The spatial symbols indicate the indexes of the active antennas, $\ell_{\Re}$ and $\ell_{\Im}$, that will be respectively used to transmit $x_{\Re}$ and $x_{\Im}$. Consequently, the transmitted N_t—dimensional vector $\mathbf{x}$ is generated, which contains only one real element and another imaginary element and the rest of the elements are set to zero.

The received signal at the destination during the first phase is given by

$$\mathbf{y}_{s-d} = \tilde{\mathbf{H}}\mathbf{x} + \mathbf{z}, \tag{5}$$

where $\mathbf{z}$ being an N_r—dimensional additive white Gaussian noise (AWGN) vector seen at the input of the destination receive antennas with entires having zero mean and σ_n^2 variance.

Likewise, the received vector at the ith relay can be expressed as

$$\mathbf{y}_{s-r}^{(i)} = \tilde{\mathbf{G}}^{(i)}\mathbf{x} + \mathbf{w}^{(i)}, \tag{6}$$

where $\mathbf{w}^{(i)}$ is the AWGN vector seen at the *ith* relay input with L_r-dimension and similar characteristics as discussed for $\mathbf{z}$.

The received signals at the relays are processed and each relay applies QSM maximum likelihood (ML) decoder to estimate the transmitted symbol as [2]

$$\hat{\mathbf{x}}^{(i)} = \arg\min_{\mathbf{x}\in\mathscr{X}} \left\| \mathbf{y}_{s-r}^{(i)} - \hat{\mathbf{G}}^{(i)}\mathbf{x} \right\|_F^2 \tag{7}$$

where $\mathscr{X}$ denotes the set of all possible transmission vectors, and $\|\cdot\|_F^2$ is the Frobenius norm. In this paper as well, it is assumed that the relay and the destination apply a channel estimation algorithm to estimate their corresponding channel entries utilizing pilot symbols transmitted by the source. As such, $\hat{\mathbf{G}}^{(i)}$ denotes the estimated version of $\tilde{\mathbf{G}}^{(i)}$ and $\hat{\mathbf{G}}^{(i)}$ and $\tilde{\mathbf{G}}^{(i)}$ are assumed to be jointly ergodic and stationary processes. In addition, assuming that the estimated channel and the estimation error are orthogonal yields,

$$\hat{\mathbf{G}}^{(i)} = \tilde{\mathbf{G}}^{(i)} + \mathbf{G}_e^{(i)} \tag{8}$$

where $\mathbf{G}_e^{(i)}$ represents the estimation error matrix whose entries are modeled by complex Gaussian random variables with zero mean and ϵ^2 variance.

2.2 Second transmission phase

In the relaying phase, only the relays that decode the source message signal correctly are allowed to participate in retransmitting the decoded signals to the destination. Let $\mathscr{C}$ denotes the set of all relays that will be active in the second phase. The relay decodes the source message and then encodes it again using QSM technique. The generated QSM signal, $\mathbf{s}$, is then transmitted from L_t antennas to the destination. It should be noted that we assume arbitrary number of transmit antennas at the relays, which is not necessarily matching the number of antennas at the source, $N_t \neq L_t$. Thereby and in order to forward the same number of bits to the destination, different modulation orders might be considered at the source and the relays. Specifically, the modulation order at the forwarding relay, M_r, should satisfy $M_r = \frac{N_t^2 M_s}{L_t^2}$.

The received signal at the destination from the $ith, i \in \{1:\mathscr{C}\}$ forwarding relay can be expressed as follows

$$\mathbf{y}_{r-d}^{(i)} = \tilde{\mathbf{F}}^{(i)}\mathbf{s} + \mathbf{n}^{(i)} \tag{9}$$

where $\mathbf{n}^{(i)}$ is the AWGN vector seen at the destination input with identical entries as discussed before for $\mathbf{w}^{(i)}$.

The destination node processes all received data from both phases to retrieve original data bits as

$$\hat{\mathbf{x}}^{d} = \arg\min_{\tilde{\mathbf{x}}\in\mathscr{X}} \left\| \mathbf{y}_{s-d} - \hat{\mathbf{H}}\tilde{\mathbf{x}} \right\|_F^2 + \sum_{i=1}^{R} \zeta_i \left\| \mathbf{y}_{r-d}^{(i)} - \hat{\mathbf{F}}^{(i)}\tilde{\mathbf{s}} \right\|_F^2 \tag{10}$$

where ζ_i is a binary variable that indicates if the relay is active, ($\zeta_i = 1$), or inactive, ($\zeta_i = 0$). It is worth mentioning that although $\tilde{\mathbf{x}}$ and $\tilde{\mathbf{s}}$ have different dimensions and elements, they both must refer to the same data block when mapped back to bits. The matrices $\hat{\mathbf{H}}$ and $\hat{\mathbf{F}}^{(i)}$ respectively represent the estimated versions of $\tilde{\mathbf{H}}$ and $\tilde{\mathbf{F}}^{(i)}$ at the destination. Besides, $\hat{\mathbf{H}}$ and $\hat{\mathbf{F}}^{(i)}$ are expressed respectively as follows

$$\hat{\mathbf{H}} = \tilde{\mathbf{H}} + \mathbf{H}_e \tag{11}$$

$$\hat{\mathbf{F}}^{(i)} = \tilde{\mathbf{F}}^{(i)} + \mathbf{F}_e^{(i)} \tag{12}$$

where $\mathbf{H}_e$ and $\mathbf{F}_e^{(i)}$ are the corresponding channel estimation error matrices with Gaussian noise random variable entries with zero mean and ϵ^2 variance.

3 Performance analysis

Performance analysis of the described system in the previous section is derived hereinafter. In particular, the average bit error rate (BER) is computed using the tight union upper bound as [20]

$$\mathrm{BER} = \frac{1}{N_t^2 M_s \log_2\left(N_t^2 M_s\right)} \sum_{\mathbf{x}\in\mathscr{X}} \sum_{\tilde{\mathbf{x}}\neq\mathbf{x}} D_{\tilde{\mathbf{x}},\mathbf{x}} \bar{P}_{\tilde{\mathbf{x}},\mathbf{x}} \tag{13}$$

where $D_{\tilde{\mathbf{x}},\mathbf{x}}$ is the hamming distance between the two symbols represented by $\tilde{\mathbf{x}}$ and $\mathbf{x}$, and $\overline{P}_{\tilde{\mathbf{x}},\mathbf{x}}$ denotes the average pairwise error probability (PEP) of $\tilde{\mathbf{x}}$ being detected given that $\mathbf{x}$ has been transmitted.

Considering the ML detector given in (10), the PEP is derived as

$$P_{\tilde{\mathbf{x}},\mathbf{x}} = \Pr\Bigg\{ \left\| \mathbf{y}_{s-d} - \hat{\mathbf{H}}\mathbf{x} \right\|_F^2 + \sum_{i=1}^{R} \zeta_i \left\| \mathbf{y}_{r-d}^{(i)} - \hat{\mathbf{F}}^{(i)}\mathbf{s} \right\|_F^2 > \left\| \mathbf{y}_{s-d} - \hat{\mathbf{H}}\tilde{\mathbf{x}} \right\|_F^2 + \sum_{i=1}^{R} \zeta_i \left\| \mathbf{y}_{r-d}^{(i)} - \hat{\mathbf{F}}^{(i)}\tilde{\mathbf{s}} \right\|_F^2 \Bigg\} \tag{14}$$

Now, substituting $\mathbf{y}_{s-d}$ from (5), $\mathbf{y}_{r-d}$ from (9), $\hat{\mathbf{H}}$ from (11) and $\hat{\mathbf{F}}^{(i)}$ from (12), and after simple mathematical manipulations leads to the simplified PEP formula given as

$$P_{\tilde{\mathbf{x}},\mathbf{x}} = \Pr\left\{ \|\mathbf{z} - \mathbf{H}_e\mathbf{x}\|_F^2 + \sum_{i=1}^{R} \zeta_i \left\| \mathbf{n}^{(i)} - \mathbf{F}_e^{(i)}\mathbf{s} \right\|_F^2 \right. \\ > \left\| \hat{\mathbf{H}}(\mathbf{x} - \tilde{\mathbf{x}}) + \mathbf{z} - \mathbf{H}_e\mathbf{x} \right\|_F^2 + \sum_{i=1}^{R} \zeta_i \\ \left. \left\| \hat{\mathbf{F}}^{(i)}(\mathbf{s} - \tilde{\mathbf{s}}) + \mathbf{n}^{(i)} - \mathbf{F}_e^{(i)}\mathbf{s} \right\|_F^2 \right\}. \tag{15}$$

Expanding all norms in (15) and canceling identical terms in both sides, (15) can be simplified to

$$2\mathrm{Re}\left\{ \hat{\mathbf{H}}(\tilde{\mathbf{x}} - \mathbf{x})(\mathbf{z} - \mathbf{H}_e\mathbf{x})^H + \sum_{i=1}^{R} \zeta_i \hat{\mathbf{F}}^{(i)}(\tilde{\mathbf{s}} - \mathbf{s})(\mathbf{n}^{(i)} - \mathbf{F}_e^{(i)}\mathbf{s})^H \right\} \\ > \left\| \hat{\mathbf{H}}(\mathbf{x} - \tilde{\mathbf{x}}) \right\|_F^2 + \sum_{i=1}^{R} \zeta_i \left\| \hat{\mathbf{F}}^{(i)}(\mathbf{s} - \tilde{\mathbf{s}}) \right\|_F^2, \tag{16}$$

where the superscript H indicates the matrix Hermitian operator, and $\mathrm{Re}\{\cdot\}$ is the real part of complex number.

For a given $\hat{\mathbf{H}}$, $\hat{\mathbf{F}}^{(i)}$ and ζ, the left-hand side of the probability in (16) is a Gaussian random variable with zero mean and variance of

$$2\left(\sigma_n^2 + \epsilon^2\right)\left(\left| \hat{\mathbf{H}}(\tilde{\mathbf{x}} - \mathbf{x}) \right|_F^2 + \sum_{i=1}^{R} \zeta_i \left| \hat{\mathbf{F}}^{(i)}(\tilde{\mathbf{s}} - \mathbf{s}) \right|_F^2 \right)$$

. Hence, the PEP in (16) can be rewritten as

$$P_{(\tilde{\mathbf{x}},\mathbf{X}/\hat{\mathbf{H}},\hat{\mathbf{F}},\zeta)} = Q\left(\sqrt{\frac{\left| \hat{\mathbf{H}}(\mathbf{x} - \tilde{\mathbf{x}}) \right|_F^2 + \sum_{i=1}^{R} \zeta_i \left| \hat{\mathbf{F}}^{(i)}(\mathbf{s} - \tilde{\mathbf{s}}) \right|_F^2}{2(\sigma_n^2 + \epsilon^2)}} \right). \tag{17}$$

where $Q(\cdot)$ denotes the Gaussian Q-function which can be expressed through Craig's formula as [21]

$$Q(a) = \frac{1}{\pi}\int_0^{\frac{\pi}{2}} \exp\left(-\frac{a^2}{2\sin\theta} \right) \cdot d\theta. \tag{18}$$

Taking the expectation of (17) over $\hat{\mathbf{H}}$ and $\hat{\mathbf{F}}^{(i)}$ yields

$$\overline{P}_{(\tilde{\mathbf{x}},\mathbf{x}/\zeta)} = \mathrm{E}\left[Q\left(\sqrt{\frac{\left| \hat{\mathbf{H}}\Delta_x \right|_F^2 + \sum_{i=1}^{R} \zeta_i \left| \hat{\mathbf{F}}^{(i)}\Delta_s \right|_F^2}{2\left(\sigma_n^2 + \epsilon^2\right)}} \right) \right] \tag{19}$$

where E denotes the expectation operator, $\Delta_x = \mathbf{x} - \tilde{\mathbf{x}}$, $\Delta_s = \mathbf{s} - \tilde{\mathbf{s}}$, and $C = \sum_{i=1}^{R} \zeta_i$.

Using (18), the Q-function in (19) can be rewritten as

$$\mathrm{E}\left[Q\left(\sqrt{\frac{\left| \hat{\mathbf{H}}\Delta_x \right|_F^2 + \sum_{i=1}^{R} \zeta_i \left| \hat{\mathbf{F}}^{(i)}\Delta_s \right|_F^2}{2(\sigma_n^2 + \epsilon^2)}} \right) \right] \\ = \frac{1}{\pi}\int_0^{\frac{\pi}{2}} \mathrm{E}\left[\exp\left(-\frac{\left| \hat{\mathbf{H}}\Delta_x \right|_F^2 + \sum_{i=1}^{R} \zeta_i \left| \hat{\mathbf{F}}^{(i)}\Delta_s \right|_F^2}{4\left(\sigma_n^2 + \epsilon^2\right)\sin\theta} \right) \right] \cdot d\theta. \tag{20}$$

As both $\hat{\mathbf{H}}$ and $\hat{\mathbf{F}}^{(i)}$ are independent, the expectation can be separated as follows

$$\mathrm{E}\left[Q\left(\sqrt{\frac{\left| \hat{\mathbf{H}}\Delta_x \right|_F^2 + \sum_{i=1}^{R} \zeta_i \left| \hat{\mathbf{F}}\Delta_s \right|_F^2}{2(\sigma_n^2 + \epsilon^2)}} \right) \right] \\ = \frac{1}{\pi}\int_0^{\frac{\pi}{2}} \mathrm{E}\left[\exp\left(\varphi \left| \hat{\mathbf{H}}\Delta_x \right|_F^2 \right) \right] \mathrm{E}\left[\exp\left(\varphi \sum_{i=1}^{R} \zeta_i \left| \hat{\mathbf{F}}\Delta_s \right|_F^2 \right) \right] \cdot d\theta \tag{21}$$

where $\varphi = \frac{-1}{4(\sigma_n^2 + \epsilon^2)\sin\theta}$. Using the Moment Generation Functions (MGF), (21) can be given as

$$\mathrm{E}\left[Q\left(\sqrt{\frac{\left| \hat{\mathbf{H}}\Delta_x \right|_F^2 + \sum_{i=1}^{R} \zeta_i \left| \hat{\mathbf{F}}\Delta_s \right|_F^2}{2\left(\sigma_n^2 + \epsilon^2\right)}} \right) \right] \\ = s\frac{1}{\pi}\int_0^{\frac{\pi}{2}} \Phi(\varphi) \prod_{i=1}^{R} \Omega(\zeta_i\varphi) \cdot d\theta = \frac{1}{\pi}\int_0^{\frac{\pi}{2}} \Phi(\varphi)(\Omega(\varphi))^C \cdot d\theta, \tag{22}$$

where Φ denotes the MGF of the variable $\left| \hat{\mathbf{H}}\Delta_x \right|_F^2$ and Ω is the MGF of the random variable $\left| \hat{\mathbf{F}}\Delta_s \right|_F^2$.

The variable C is the cardinality of the set $\mathscr{C}$, which indicates the number of relays that successfully decoded the source signal correctly and will participate in the second communication phase. Therefore, it is a binomial random variable with probability δ given by

$$\delta = \mathrm{E}\left[Q\left(\sqrt{\frac{\left| \hat{\mathbf{G}}(\mathbf{x} - \tilde{\mathbf{x}}) \right|_F^2}{2\left(\sigma_n^2 + \varepsilon^2\right)}} \right) \right] = \mathrm{E}\left[Q\left(\sqrt{\frac{\left| \hat{\mathbf{G}}\Delta_x \right|_F^2}{2\left(\sigma_n^2 + \varepsilon^2\right)}} \right) \right], \tag{23}$$

which indicates the average PEP at each relay. Following similar steps as discussed when obtaining (20)–(22), δ can be written in terms of the MGF as

$$\delta = \frac{1}{\pi}\int_0^{\frac{\pi}{2}} \beta(\varphi) \cdot d\theta, \tag{24}$$

with β denoting the MGF of the variable $|\mathbf{G}\Delta_x|_F^2$.

Using (22) and (24), the average PEP can be expressed as follows

$$\bar{P}_{\tilde{\mathbf{x}},\mathbf{x}} = \sum_{C=1}^{R} \binom{C}{R} \delta^{R-C}(1-\delta)^{C} \frac{1}{\pi}\int_{0}^{\frac{\pi}{2}} \Phi(\varphi)(\Omega(\varphi))^{C} \cdot d\theta. \tag{25}$$

According to [22], the variable $\left|\hat{\mathbf{H}}\Delta_x\right|_F^2$ can be expanded as

$$\begin{aligned}\left|\hat{\mathbf{H}}\Delta_x\right|_F^2 &= \mathrm{trace}\{\hat{\mathbf{H}}\Delta_x\Delta_x^H\hat{\mathbf{H}}^H\}\\ &= \mathrm{vec}\left(\mathbf{H}^H\right)^H \mathbf{R}_{\mathbf{H}}^{\frac{H}{2}}(\mathbf{I}_{N_r}\otimes\Delta_x\Delta_x^H)\mathbf{R}_{\mathbf{H}}^{\frac{1}{2}}\mathrm{vec}(\mathbf{H}^H)\\ &= \mathbf{H}_v{}^H\psi_x\mathbf{H}_v,\end{aligned} \tag{26}$$

where trace is the matrix trace operator, $\mathrm{vec}(\cdot)$ is the vectorization operator, and $\otimes$ denotes the Kronecker product. Also, $\psi_x = (\mathbf{I}_{N_r}\otimes\Delta_x\Delta_x^H)$, $\mathbf{R}_{\mathbf{H}} = \mathbf{R}_d\otimes\mathbf{R}_s$ and $\mathbf{H}_v = \mathbf{R}_{\mathbf{H}}^{\frac{1}{2}}\mathrm{vec}(\mathbf{H}^H)$. Following the same approach in (26), the parameters $\left|\hat{\mathbf{F}}\Delta_s\right|_F^2$ and $\left|\hat{\mathbf{G}}\Delta_x\right|_F^2$ can be respectively given as

$$\left|\hat{\mathbf{F}}\Delta_s\right|_F^2 = \mathbf{F}_v{}^H\psi_s\mathbf{F}_v \tag{27}$$

$$\left|\hat{\mathbf{G}}\Delta_x\right|_F^2 = \mathbf{G}_v{}^H\psi_g\mathbf{G}_v \tag{28}$$

where $\psi_s = (\mathbf{I}_{N_r}\otimes\Delta_s\Delta_s^H)$, $\psi_g = (\mathbf{I}_{L_r}\otimes\Delta_x\Delta_x^H)$, $\mathbf{F}_v = \mathbf{R}_{\mathbf{F}}^{\frac{1}{2}}\mathrm{vec}(\mathbf{F}^H)$, $\mathbf{G}_v = \mathbf{R}_{\mathbf{G}}^{\frac{1}{2}}\mathrm{vec}(\mathbf{G}^H)$, $\mathbf{R}_{\mathbf{F}} = \mathbf{R}_d\otimes\mathbf{R}_{rt}$, and $\mathbf{R}_{\mathbf{G}} = \mathbf{R}_{rr}\otimes\mathbf{R}_s$.

The MGFs for the variables in (26), (27) and (28) are respectively written using the quadratic form solution as [23]

$$\Phi(\varphi) = \frac{\exp\left(\varphi\overline{\mathbf{H}}^H\psi_x(\mathbf{I}_{N_rN_t}-\varphi\mathbf{V}_{\mathbf{H}}\psi_x)^{-1}\overline{\mathbf{H}}\right)}{\det(\mathbf{I}_{N_rN_t}-\varphi\mathbf{V}_{\mathbf{H}}\psi_x)} \tag{29}$$

$$\Omega(\varphi) = \frac{\exp\left(\varphi\overline{\mathbf{F}}^H\psi_s(\mathbf{I}_{N_rL_t}-\varphi\mathbf{V}_{\mathbf{F}}\psi_s)^{-1}\overline{\mathbf{F}}\right)}{\det(\mathbf{I}_{N_rL_t}-\varphi\mathbf{V}_{\mathbf{F}}\psi_s)} \tag{30}$$

$$\beta(\varphi) = \frac{\exp\left(\varphi\overline{\mathbf{G}}^H\psi_g\left(\mathbf{I}_{L_rN_t}-\varphi\mathbf{V}_{\mathbf{G}}\psi_g\right)^{-1}\overline{\mathbf{G}}\right)}{\det\left(\mathbf{I}_{L_rN_t}-\varphi\mathbf{V}_{\mathbf{G}}\psi_g\right)} \tag{31}$$

where $\overline{\mathbf{H}}$, $\overline{\mathbf{F}}$ and $\overline{\mathbf{G}}$ are the mean vectors of $\mathbf{H}_v$, $\mathbf{F}_v$ and $\mathbf{G}_v$, respectively, and $\mathbf{V}_{\mathbf{H}}$, $\mathbf{V}_{\mathbf{F}}$ and $\mathbf{V}_{\mathbf{G}}$ respectively denote the covariance matrices of $\mathbf{H}_v$, $\mathbf{F}_v$ and $\mathbf{G}_v$.

Now, plugging (29) and (30) in (22), the resultant integral can be upper bounded as follows

$$\begin{aligned}&\frac{1}{\pi}\int_0^{\frac{\pi}{2}}\Phi(\varphi)(\Omega(\varphi))^C\cdot d\theta \leqslant\\ &\frac{1}{2}\frac{\left(\exp\alpha\overline{\mathbf{H}}^H\psi_x(\mathbf{I}_{N_rN_t}-\alpha\mathbf{V}_{\mathbf{H}}\psi_x)^{-1}\overline{\mathbf{H}}\right)}{\det(\mathbf{I}_{N_rN_t}-\alpha\mathbf{V}_{\mathbf{H}}\psi_x)}\times\\ &\left(\frac{\exp\left(\alpha\overline{\mathbf{F}}^H\psi_s(\mathbf{I}_{N_rL_t}-\alpha\mathbf{V}_{\mathbf{F}}\psi_s)^{-1}\overline{\mathbf{F}}\right)}{\det(\mathbf{I}_{N_rL_t}-\alpha\mathbf{V}_{\mathbf{F}}\psi_s)}\right)^C\end{aligned} \tag{32}$$

where $\alpha = \frac{-1}{4(\sigma_n^2+\epsilon^2)}$. Consequently, (32) is substituted in (25) to obtain the average pairwise error probability at the destination as

$$\begin{aligned}\bar{P}_{\tilde{\mathbf{x}},\mathbf{x}} \leqslant &\frac{1}{2}\sum_{C=1}^{R}\binom{C}{R}\delta^{R-C}(1-\delta)^C\\ &\left[\frac{\exp\left(\alpha\overline{\mathbf{H}}^H\psi_x(\mathbf{I}_{N_rN_t}-\alpha\mathbf{V}_{\mathbf{H}}\psi_x)^{-1}\overline{\mathbf{H}}\right)}{\det(\mathbf{I}_{N_rN_t}-\alpha\mathbf{V}_{\mathbf{H}}\psi_x)}\right.\\ &\left.\times\left(\frac{\exp\left(\alpha\overline{\mathbf{F}}^H\psi_s(\mathbf{I}_{N_rL_t}-\alpha\mathbf{V}_{\mathbf{F}}\psi_s)^{-1}\overline{\mathbf{F}}\right)}{\det(\mathbf{I}_{N_rL_t}-\alpha\mathbf{V}_{\mathbf{F}}\psi_s)}\right)^C\right],\end{aligned} \tag{33}$$

where δ can be also given as an upper bound of the integral in (24) after substituting (31) as

$$\delta \leqslant \frac{1}{2}\frac{\exp\left(\alpha\overline{\mathbf{G}}^H\psi_g\left(\mathbf{I}_{L_rN_t}-\alpha\mathbf{V}_{\mathbf{G}}\psi_g\right)^{-1}\overline{\mathbf{G}}\right)}{\det\left(\mathbf{I}_{L_rN_t}-\alpha\mathbf{V}_{\mathbf{G}}\psi_g\right)}. \tag{34}$$

Finally, plugging (34) in (33), and then in (13), the average BER at the destination can be computed. However, the mean and the variance of the three fading channel links (i.e, $\mathbf{H}$, $\mathbf{F}$ and $\mathbf{G}$) are required to compute the average BER. Considering the η–μ fading channels, the mth moment of the channel, denoted by $\mathrm{E}[P^m]$, is given by [24, 25]

$$\begin{aligned}\mathrm{E}[P^m]_{\eta-\mu} = &\frac{(1-\eta^2)^{\mu+\frac{m}{2}}\Gamma\left(2\mu+\frac{m}{2}\right)}{(2\mu)^{\frac{m}{2}}\Gamma(2\mu)}\\ &\times {}_2F_1\left(\mu+\frac{1}{2},\frac{m}{4},\mu+\frac{m}{4};\mu_{\frac{1}{2}};\eta^2\right)\end{aligned} \tag{35}$$

where $\Gamma(\cdot)$ is the gamma function and ${}_2F_1(\cdot)$ is the Gauss hypergeometric function [26, Eq. 15.1.1].

Accordingly, $\overline{\mathbf{H}}$, $\overline{\mathbf{F}}$ and $\overline{\mathbf{G}}$ are respectively given by

$$\overline{\mathbf{H}} = \mathrm{E}[P]\mathbf{R}_{\mathbf{H}}^{\frac{1}{2}}\mathrm{vec}(\mathbf{1}_{N_r\times N_t}) \tag{36}$$

$$\overline{\mathbf{F}} = \mathrm{E}[P]\mathbf{R}_{\mathbf{F}}^{\frac{1}{2}}\mathrm{vec}(\mathbf{1}_{N_r\times L_t}) \tag{37}$$

$$\overline{\mathbf{G}} = \mathrm{E}[P]\mathbf{R}_{\mathbf{G}}^{\frac{1}{2}}\mathrm{vec}(\mathbf{1}_{L_r\times N_t}) \tag{38}$$

where $\mathbf{1}$ is an all-ones matrix. Likewise, the covariance matrices, $\mathbf{V}_{\mathbf{H}}$, are given by

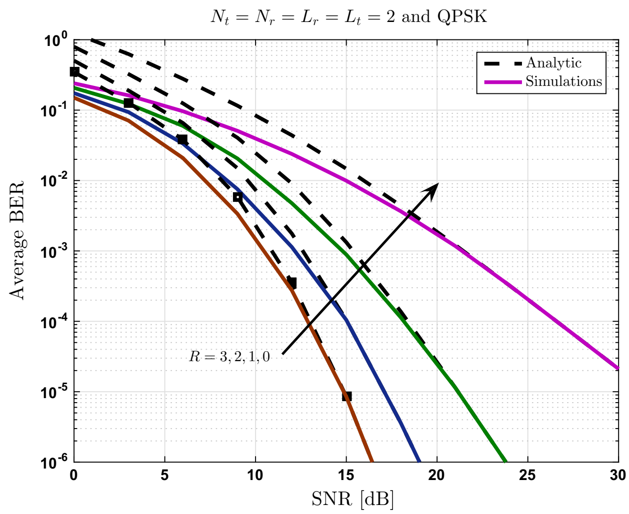

Fig. 2 Analytical and simulation average BER versus the average SNR for different number of DF relays, $R \rightarrow 0, 1, 2,$ and3, assuming $N_t = L_t = L_r = N_r = 2$, $M_s = M_r = 4-$PSK), $\eta = 1$ and $\mu = 0.5$

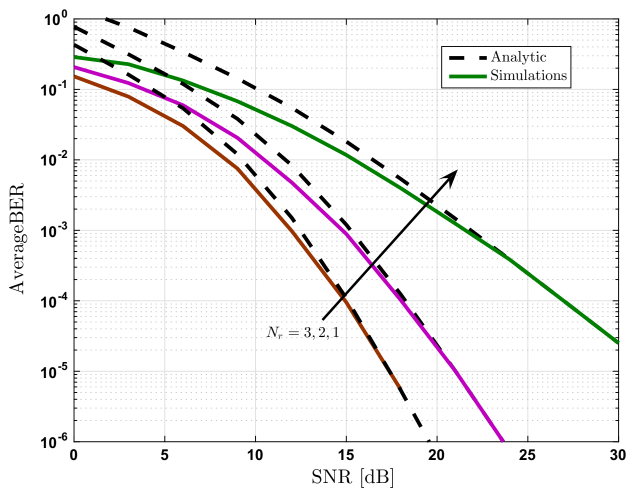

Fig. 3 The average BER versus the average SNR for different values of $N_r \rightarrow 1, 2,$ and3 and with $N_t = L_t = L_r = 2$, $R = 1$, $M_s = M_r = 4-$PSK, $\eta = 1$ and $\mu = 0.5$

$$\mathbf{V_H} = (\mathrm{E}[P^2] - \mathrm{E}^2[P])\mathbf{R_H} + \epsilon^2 \mathbf{I}_{N_r N_t} \tag{39}$$

$$\mathbf{V_F} = (\mathrm{E}[P^2] - \mathrm{E}^2[P])\mathbf{R_F} + \epsilon^2 \mathbf{I}_{N_r L_t} \tag{40}$$

$$\mathbf{V_G} = (\mathrm{E}[P^2] - \mathrm{E}^2[P])\mathbf{R_G} + \epsilon^2 \mathbf{I}_{L_r N_t} \tag{41}$$

4 Results

Monte Carlo simulation results are presented in this section to validate the conducted analysis and evaluate the performance of the proposed cooperative system. Different system configurations and channel parameters including the impact of spatial correlation and channel estimation errors are considered in the study. For Monte Carlo simulations, at least 10^6 bits are transmitted for each depicted SNR value. A Pseudo code for computing the BER is illustrated in Algorithm 1.

Algorithm 1: Pseudo code for BER computing

Initialization: Set $N_t, N_r, M_s, R, L_t, L_r, M_r, \eta, \mu, \rho, \varepsilon^2$, SNR, ;
Start ;
for *each iteration* **do**
 ——————First phase——————
 Source transmits $N_t^2 M_s$ bits.
 Generate $\widehat{\mathbf{G}}$ $\widehat{\mathbf{F}}$, $\widehat{\mathbf{H}}$, $\mathbf{z}$, $\mathbf{w}$, $\mathbf{n}$.
 Compute $\mathbf{Y}_{s-d}$ based on (5).
 Compute $\mathbf{Y}_{s-r}^{(i)}$ based on (6).
 All relays obtain the detected symbol based on (7).
 —————— Second phase ——————
 Relays that successfully detected the bits forward them to the destination.
 Compute $\mathbf{Y}_{r-d}^{(i)}$ from each forwarding relay based on (9).
 Destination uses $\mathbf{Y}_{s-d}$ and $\mathbf{Y}_{r-d}^{(i)}$ to detect the bits based on (10).
 Count the number of erroneously detected bits, and store it.
end
Compute BER as the ratio of the total erroneous bits to the total transmitted bits.

In the first results shown in Fig. 2, the average BER at the destination node versus the average SNR is studied for different number of DF relays, R. Assuming the source transmits with power E_s and the relays transmit with power E_r, the overall SNR at the destination node is given by SNR $= (E_s + E_r)/(2\sigma_n^2)$ and $\sigma_n^2 = 1/E_s$. The case of $R = 0$ corresponds to the scenario that no relays are present and communication through direct link is only available between the source and the destination. In this figure, $\eta = 1$ and $\mu = 0.5$ are considered, which corresponds to the special case of Rayleigh fading channel. Increasing the number of relays enhances the performance significantly due to the achieved diversity gain. For instance, placing a single DF relay between the source and the destination, $R = 1$, enhances the BER performance by about 8 dB at a BER of 10^{-4} as compared to the case of no relays, $R = 0$. Also, a gain of 4 dB in SNR at the same BER can be noticed when comparing the results of $R = 1$ and $R = 2$. Besides, depicted analytical and simulation results are shown to match closely for BER ¡10^{-3} and for different number of DF relays, which corroborates the accuracy of the conducted analysis.

The impact of increasing the number of receive antennas, N_r, on the overall performance is studied and the results are illustrated in Fig. 3. Similar configurations as considered in Fig. 2 are assumed here as well for $R = 1$ and only N_r varies from 1→ 3. Again, the accuracy of the derived formulas is evident from the figure and the analytical curves closely match simulation results at a asymptotically high SNR values. It is also demonstrated that increasing N_r significantly enhances the performance

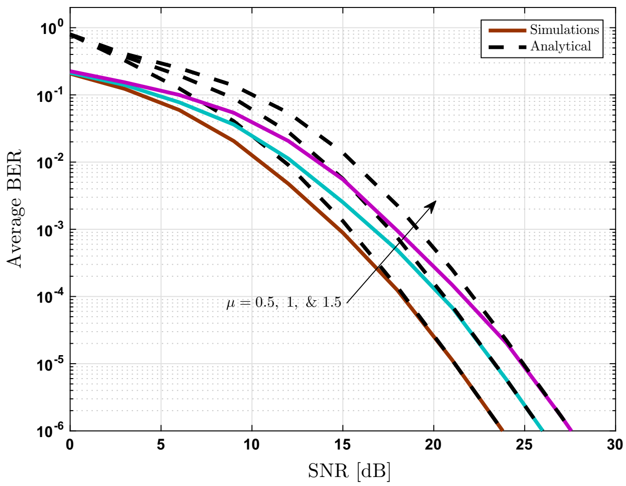

Fig. 4 The average BER versus the average SNR for different values of $\mu \to 0.5, 1, \text{and} 1.5$ assuming $N_t = L_t = L_r = N_r = 2$, $R = 1$, $M_s = M_r = 4 - \text{PSK}$ and $\eta = 1$

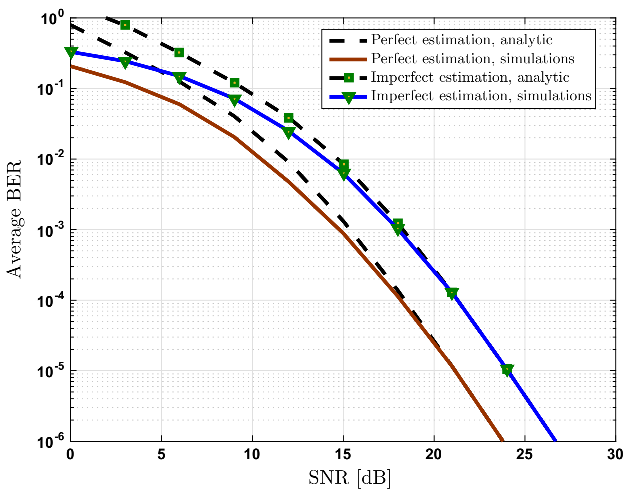

Fig. 5 The impact of channel estimation error on the overall average BER for the system under study assuming $N_t = L_t = L_r = N_r = 2$, $R = 1$, $M_s = M_r = 4 - \text{PSK}$, $\eta = 1$, and $\mu = 0.5$

and a gain of about 10 dB at a BER of 10^{-4} can be seen when increasing N_r from 1 to 2.

The impact of varying the channel parameter μ on the performance of the cooperative system under study is illustrated in Fig. 4. Recall that μ represents the number of multipaths in each cluster in the fading channel. Increasing μ results in a highly correlated channel environment and as $\mu \to \infty$, the η–μ channel becomes Gaussian and spatial multiplexing MIMO communication would be impossible since resolving different channel paths would be impossible. As such, increasing μ degrades the performance significantly and performance degradation of about 2 dB can be seen when increasing μ from 0.5 to 1.

The results shown in Fig. 5 study the impact of imperfect channel knowledge on the overall system performance.

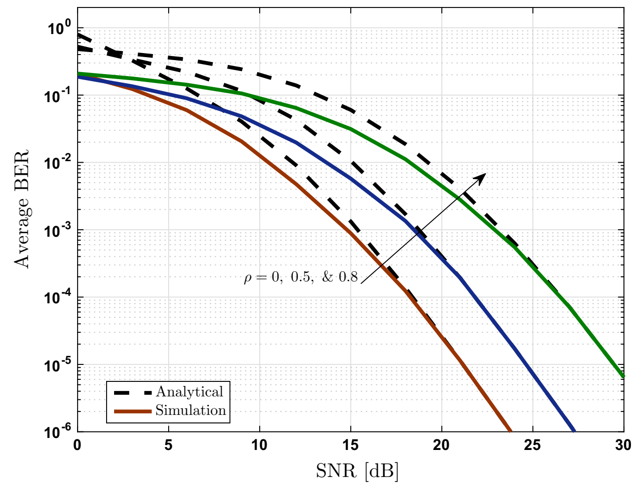

Fig. 6 The impact of spatial correlation on the overall system BER performance. Different values of $\rho \to 0, 0.5, \text{and} 0.8$ and with $N_t = L_t = L_r = N_r = 2$, $R = 1$, $M_s = M_r = 4 - \text{PSK})$, $\eta = 1$ and $\mu = 0.5$

Similar to previous studies, analytical results are shown to follow the slope of the simulation results and close match can be see at arbitrary high SNR values. A performance loss of about 3 dB due to the channel estimation errors is reported and is approximately constant for the whole considered SNR range.

All previous results are for the case of uncorrelated channel paths. Spatial correlation among transmit and/or receive antennas is anticipated to degrade the overall performance of the system as illustrated in Fig. 6. For the sake of simplicity and without loss of generality, the correlation coefficients among all antennas are assumed to be identical (i.e., $\rho_s = \rho_d = \rho_{rt} = \rho_{rr} = \rho$). The average BER curves

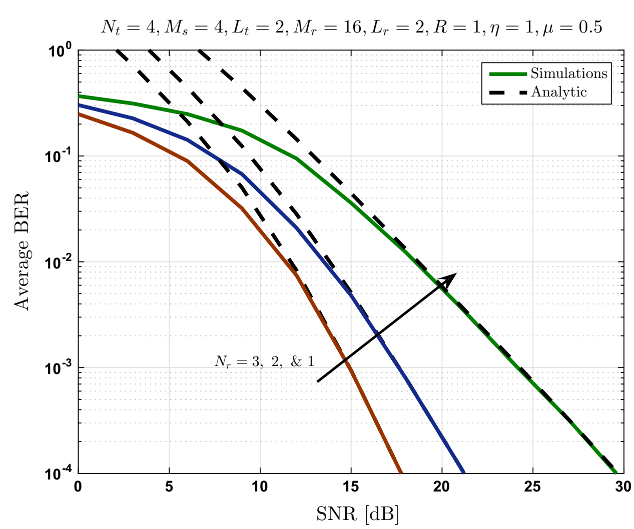

Fig. 7 The average BER versus the average SNR for unbalanced system configuration assuming $N_t = 4, L_t = L_r = 2$, $R = 1$, $M_s = 4 - \text{PSK}$, $M_r = 16 - 16 - \text{PSK}$, $\eta = 1$ and $\mu = 0.5$ and for different values of $N_r \to 1, 2,$ and 3

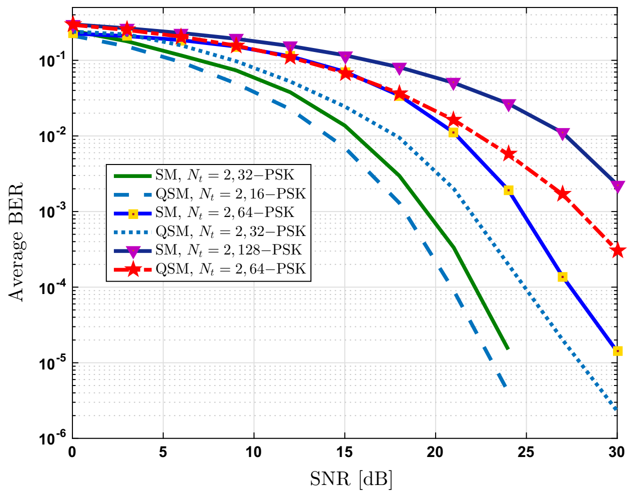

Fig. 8 QSM and SM performance comparison for spectral efficiencies of 6, 7 and 8 bits/s/Hz and with $N_r = 4, L_t = L_r = 2$, $R = 1$, $\rho = 0$, $\eta = 1$ and $\mu = 0.5$

for $\rho = 0, 0.5$ and 0.8 are depicted assuming $\eta = 1$, $\mu = 0.5$, $R = 1$, $N_t = L_t = L_r = N_r = 2$ and $M_s = M_r = 4$–PSK. As expected, spatial correlation degrades the performance of the system and with $\rho = 0.5$, 3.5 dB more SNR is required to achieve a BER $= 10^{-4}$ as compared to the uncorrelated case, $\rho = 0$.

The next study considers different configurations at the source and the relays. In all previous studies, $N_t = L_t$ and $M_s = M_r$ are assumed. In Fig. 7, we validate the derived formulas by considering different system configurations at the source and the relays. For illustration purposes, $N_t = 4$, $M_s = 4 - \text{PSK}$, and $L_t = 2$ are assumed. Hence, the relays must use a modulation order of $M_r = 16 - \text{PSK}$ in order to forward the same number of decoded bits to the destination. Analytical and simulation results for the average BER versus the average SNR at different values of $N_r \rightarrow 1, 2, \text{and} 3$ for this unbalanced system are shown match closely as depicted in Fig. 7.

Finally, comparing the performance of QSM and SM for the considered DF cooperative networks is studied and results are depicted in Fig. 8. The average BER versus the average SNR for QSM and SM schemes at different spectral efficiencies (6, 7 and 8 bits) while fixing the number of transmit antennas to $N_t = 2$ are depicted. The modulation order is adapted to achieve the target spectral efficiency for both schemes. In all depicted results, QSM demonstrates superior performance as compared to SM system and gains in SNR of about 1, 3 and 4 dB are reported at a BER $= 10^{-3}$ for 6, 7 and 8 bits spectral efficiencies, respectively, as compared to SM system. It should be noted that these enhancements come at no additional cost as QSM and SM are shown previously in [2] to require single RF-chain transmitter and similar receiver computation complexity.

5 Conclusions

This paper analyzed the performance of cooperative MIMO communication wireless system applying QSM technique at the transmitting nodes over generalized η–μ fading channels in the presence of spatial correlation and imperfect channel estimation. A closed-form upper-bound expression for the PEP is derived and used to provide an upper bound on the average BER of the system under study, which is shown to be accurate for different system and channel parameters. Obtained results reveal that channel estimation error, spatial correlation and higher μ values significantly degrade the overall performance of the system. The η–μ channel facilitates the performance evaluation over other well-known channels such as Rayleigh and Nakagami-*m*. Evaluating the capacity, mutual information and throughput of the considered system in this paper is very interesting topic to be addressed in future studies.

References

1. Wang, C. X., Haider, F., Gao, X., You, X. H., Yang, Y., Yuan, D., et al. (2014). Cellular architecture and key technologies for 5G wireless communication networks. *IEEE Communications Magazine*, *52*(2), 122–130.
2. Mesleh, R., Ikki, S. S., & Aggoune, H. M. (2015). Quadrature spatial modulation. *IEEE Transactions on Vehicular Technology*, *64*(6), 2738–2742.
3. Mesleh, R. Y., Haas, H., Sinanovic, S., Ahn, C. W., & Yun, S. (2008). Spatial modulation. *IEEE Transactions on Vehicular Technology*, *57*(4), 2228–2241.
4. Yigit, Z., & Basar, E. (2016). Low-complexity detection of quadrature spatial modulation. *Electronics Letters*, *52*(20), 1729–1731.
5. Xiao, L., Yang, P., Fan, S., Li, S., Song, L., & Xiao, Y. (2016). Low-complexity signal detection for large-scale quadrature spatial modulation systems. *IEEE Communications Letters*, *20*(11), 2173–2176.
6. Afana, A., Mahady, I. A., & Ikki, S. (2016). Quadrature spatial modulation in MIMO cognitive radio systems with imperfect channel estimation and limited feedback. IEEE Transactions on Communications.
7. Mesleh, R., Ikki, S. S., & Badarneh, O. S. (2016). Impact of cochannel interference on the performance of quadrature spatial modulation MIMO systems. *IEEE Communications Letters*, *20*(10), 1927–1930.
8. Mesleh, R., & Ikki, S. S. (2015, March). On the impact of imperfect channel knowledge on the performance of quadrature spatial modulation. In Wireless Communications and Networking Conference (WCNC), 2015 IEEE (pp. 534–538). IEEE.
9. Younis, A., Mesleh, R., & Haas, H. (2016). Quadrature spatial modulation performance over Nakagami-*m* fading channels.

IEEE Transactions on Vehicular Technology, *65*(12), 10227–10231.
10. Badarneh, O. S., & Mesleh, R. (2016). A comprehensive framework for quadrature spatial modulation in generalized fading scenarios. *IEEE Transactions on Communications*, *64*(7), 2961–2970.
11. Afana, A., Mesleh, R., Ikki, S., & Atawi, I. E. (2016). Performance of quadrature spatial modulation in amplify-and-forward cooperative relaying. *IEEE Communications Letters*, *20*(2), 240–243.
12. Afana, A., Ikki, S., Mesleh, R., & Atawi, I. (2016). Spectral efficient quadrature spatial modulation cooperative AF spectrum-sharing systems. IEEE Transactions on Vehicular Technology.
13. Afana, A., Erdogan, E., & Ikki, S. (2016, December). Quadrature spatial modulation for cooperative MIMO 5G wireless networks. In *Globecom Workshops (GC Wkshps)*, 2016 IEEE (pp. 1–5). IEEE.
14. Yacoub, M. D. (2007). The distribution and the distribution. *IEEE Antennas and Propagation Magazine*, *49*(1), 68–81.
15. Genc, V., Murphy, S., Yu, Y., & Murphy, J. (2008). IEEE 802.16 J relay-based wireless access networks: An overview. *IEEE Wireless Communications*, *15*(5),
16. Beaulieu, N. C., & Hu, J. (2006). A closed-form expression for the outage probability of decode-and-forward relaying in dissimilar Rayleigh fading channels. *IEEE Communications Letters*, *10*(12),
17. Ikki, S. S., & Ahmed, M. H. (2010). Performance analysis of adaptive decode-and-forward cooperative diversity networks with best-relay selection. *IEEE Transactions on Communications*, *58*(1),
18. Kermoal, J. P., Schumacher, L., Pedersen, K. I., Mogensen, P. E., & Frederiksen, F. (2002). A stochastic MIMO radio channel model with experimental validation. *IEEE Journal on Selected Areas in Communications*, *20*(6), 1211–1226.
19. Van Zelst, A., & Hammerschmidt, J. S. (2002). A single coefficient spatial correlation model for multiple-input multiple-output (MIMO) radio channels. In *27th general assembly of the International Union of Radio Science (URSI), Maastricht, the Netherlands* (1461–1465).
20. Proakis, J. G. (1995). *Digital communications*. New York: McGraw Hill.
21. Craig, J. W. (1991). A new, simple and exact result for calculating the probability of error for two-dimensional signal constellations. In *Military communications conference, 1991. MILCOM'91, conference record, military communications in a changing world*,. IEEE (pp. 571–575). IEEE.
22. Simon, M.K., & Alouini, M., (2005). *Digital communication over fading channels* (2nd ed.). Wiley series in telecommunications and signal processing. Wiley. ISBN: 978-0-471-64953-3.
23. Turin, G. L. (1960). The characteristic function of Hermitian quadratic forms in complex normal variables. *Biometrika*, *47*(1/2), 199–201.
24. Yacoub, M. D. (2007). The distribution and the distribution. *IEEE Antennas and Propagation Magazine*, *49*(1), 68–81.
25. Papazafeiropoulos, A. K., & Kotsopoulos, S. A. (2009, September). The joint envelope-phase fading distribution. In *2009 IEEE 20th international symposium on personal, indoor and mobile radio communications* (pp. 919–922). IEEE.
26. Abramnowitz, M., & Stegun, I. A. (1972). *Handbook of mathematical functions*. Washington, DC: US Dept. of Commerce, National Bureau of Standards.

Saud Althunibat received his Ph.D. degree in Telecommunications from the University of Trento (Italy) in 2014. Currently, he is an assistant professor at Al-Hussein Bin Talal University (Jordan). He has authored more than 40 scientific papers. He has received the best paper award in IEEE CAMAD 2012, and was selected as Exemplary Reviewer for IEEE Communications Letters in 2013. He is a regular reviewer in many journals, and a TPC member in many international conferences. His research interests include physical-layer security, space modulation, cognitive radio, wireless sensor networks and resource allocation.

Raed Mesleh is currently the vice dean of the School of Electrical Engineering and Information Technology at German Jordanian University in Amman, Jordan. He received his Ph.D. in 2007 from Jacobs University in Bremen, Germany. From 2007 to 2010 he was a postdoctoral fellow at Jacobs University. He was with the Electrical Engineering Department at University of Tabuk in Saudi Arabia from 2010 to 2015. During that period, he holds the position of department chair and the director of research excellence and intellectual property units at the deanship of scientific research. He was a visiting scholar at Boston University, The University of Edinburgh and Heriot-Watt University. He received the Arab Scientific Creativity Award from Arab thought Foundations in December 2016. His main research interests are in wireless communication and optical wireless communication with particular focus on MIMO techniques, mmWave communication FSO and VLC. He is an inventor and co-inventor of seven patents, three of them are already granted, and published more than 100 journal and conference papers.